Stability of DNA-linked nanoparticle crystals: Effect of number of strands, core size, and rigidity of strand attachment

Olivia Padovan-Merhar,[a] Fernando Vargas Lara,[b] and Francis W. Starr
Department of Physics, Wesleyan University, Middletown, Connecticut 06459, USA

(Received 4 March 2011; accepted 11 May 2011; published online 22 June 2011)

Three-dimensional ordered lattices of nanoparticles (NPs) linked by DNA have potential applications in novel devices and materials, but most experimental attempts to form crystals result in amorphous packing. Here we use a coarse-grained computational model to address three factors that impact the stability of bcc and fcc crystals formed by DNA-linked NPs : (i) the number of attached strands to the NP surface, (ii) the size of the NP core, and (iii) the rigidity of the strand attachment. We find that allowing mobility in the attachment of DNA strands to the core NP can very slightly increase or decrease melting temperature T_M. Larger changes to T_M result from increasing the number of strands, which increases T_M, or by increasing the core NP diameter, which decreases T_M. Both results are consistent with experimental findings. Moreover, we show that the behavior of T_M can be quantitatively described by the model introduced previously [F. Vargas Lara and F. W. Starr, Soft Matter, **7**, 2085 (2011)]. © *2011 American Institute of Physics*. [doi:10.1063/1.3596745]

I. INTRODUCTION

DNA is a programmable molecule with four nucleotide types that can selectively and reversibly bind; the DNA double helix has a diameter of 2 nm and is relatively stiff, with a persistence length of $\approx$60 nm.[1] These features make DNA a promising mediator for the "bottom-up" assembly of nanostructured materials.[2–7] One method to realize DNA-linked materials is to tether single strands of DNA (ssDNA) to a "hub," such as a colloid[8–17] or nanoparticle (NP).[4,5,18–32] Through the appropriate choice of nucleotide sequence, ssDNA tethered to different NPs can hybridize to make double-stranded DNA (dsDNA) that link complex networks of NPs. In particular, crystalline arrays of NPs have potential applications in novel optical and electronic devices and materials, and have been an ongoing focus of experimental efforts.[33] While some experimental success has been achieved in synthesizing DNA-linked crystals,[24,28–32,34] most attempts to form such structures result in amorphous packing.

There are many factors that affect crystal formation and the stability of the resulting structure, such as the DNA strand length and sequence, the size of the NP core, and the number of attached strands to the NP, to name a few. Testing each of these factors individually in a laboratory is time consuming and, in some cases, not feasible. However, with a computational model, it is relatively straightforward to vary such parameters and observe the effect each has on crystal stability. The first paper in this series[35] examined the effect of the strand length and nucleotide sequence on crystal stability based on a coarse-grained molecular model of DNA-functionalized NPs. In this paper, we slightly modify the model in Ref. 35 to examine how crystal stability is affected by rigidity of the DNA attachment to the NP surface, variable numbers of DNA strands attached to the NP core, and variable NP core size.

We find that modest mobility of the ssDNA attachment to the core NP can either increase or decrease the melting temperature T_M relative to a system with rigidly attached DNA strands, but that the effect is weak. The sign of the change in T_M is determined by whether the geometry of rigidly attached strands matches the local crystal order. By varying the number of ssDNA attached to a NP, we show that T_M of crystals generally increases with the number of attached strands, due to the possibility for multiple DNA links to cooperatively form between NPs. By varying the NP core size, we find that T_M generally decreases with an increasing NP size. We interpret all our results using the model for T_M previously. We confirm that this model accounts for the behavior of T_M found in this work. The applicability of the model is limited to the cases of strands shorter than the persistence length and where the melting of the crystal is dominated by the DNA zipper transition. For very densely functionalized NP, the particles act more like soft spheres reducing the importance of the DNA specific binding.[36] Initial comparisons with experimental data indicate consistency with our model.

II. MODEL AND SIMULATION METHODS

Atomistic simulations of DNA-functionalized NPs represent a major computational challenge. For example, a recent state-of-the-art atomistic study considered only a single NP functionalized with four 10-base DNA strands.[37] Accordingly, using an atomistic model to simulate the interactions between tens or hundreds of DNA-functionalized NPs for timescales commensurate with DNA zipping is difficult, if not impossible, with current computational resources. Therefore, we use a coarse-grained model to study many NPs on timescales long enough to observe the reorganization

[a]Present address: Department of Physics and Astronomy, University of Pennsylvania, Philadelphia, Pennsylvania 19104-6396, USA.
[b]Author to whom correspondence should be addressed. Electronic mail: lvargaslara@wesleyan.edu and fstarr@wesleyan.edu.

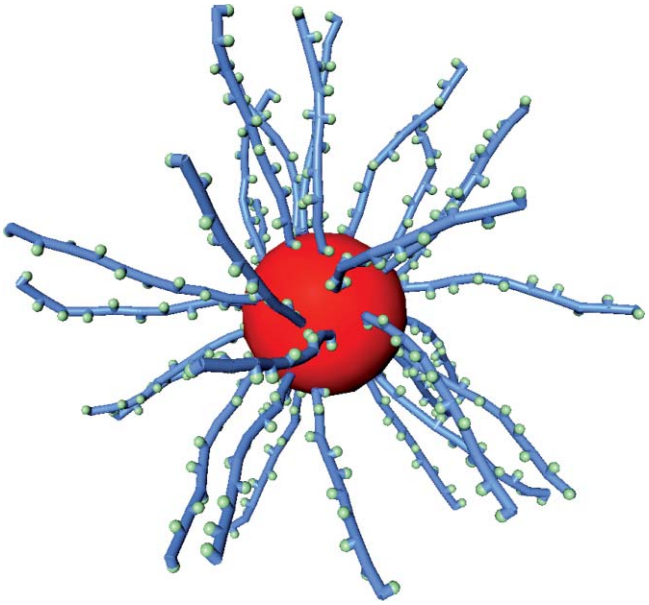

FIG. 1. Snapshot of the spherical-core model with 30 DNA "arms". The large central red sphere represents the core NP. The blue cylinders represent the bonds between the backbone monomers (not pictured). The small green spheres are the "sticky spots" which carry A/C/G/T identity. The simplicity of this model allows for a variable number of strands attached to an NP of variable size.

necessary to melt crystalline ordered NPs linked by DNA. The model includes the specificity of DNA base-pair binding, but excludes effects due to specific chemical or solution interactions. This model has been shown to capture the relevant features of DNA-mediated assembly.[38–42] The model we use is an adaptation of the model used to study icosahedral NP functionalized with DNA.[35]

In this model, each DNA nucleotide consists of two force sites: one represents the sugar-phosphate backbone of DNA (monomer), and one carries the A/C/G/T identity of the nitrogenous base (sticky site). Details of the DNA potential can be found in Refs. 35, 43, and 44. Since the atomistic structure of a gold NP core (commonly used in experiments) is highly symmetric, we expect the detailed NP structure plays little role in crystal stability. In Ref. 35, the NP core was treated as a collection of "atoms" in an icosahedral geometry; here, we further simplify by modeling the core NP as a single spherically symmetric particle (Fig. 1). To allow us to easily vary the core size without changing the scale of the interactions, we use a repulsive Weeks-Chandler-Andersen (WCA) potential for the core NP where we shift the origin, namely

$$U_{\mathrm{WCA}}^{\mathrm{core}}(r) = U_{\mathrm{LJ}}(r - r_s) - U_{\mathrm{LJ}}(r_c) - (r - r_c)\left.\frac{dU_{\mathrm{LJ}}(r - r_c)}{dr}\right|_{r=r_c}, \tag{1}$$

where U_{LJ} is the Lennard-Jones (LJ) potential, r is the separation between the core NP and another force site, r_s is the amount by which the origin is shifted, and r_c is a cutoff distance for the potential. By shifting the origin in such a manner, and choosing $r_c = r_s + 2^{1/6}\sigma$ (σ is the LJ length parameter), corresponding to the minimum of the shifted-origin potential, the core can be thought of as a WCA particle with radius $r_{\mathrm{core}} = r_s + \frac{\sigma}{2}$, and diameter $d = 2r_{\mathrm{core}}$.

The first monomer of each DNA strand is attached to the core via an origin shifted finitely extensible nonlinear elastic (FENE) bond potential,

$$U_{\mathrm{FENE}}^{\mathrm{core}}(r) = -\frac{kR_0^2}{2}\ln\left[1 - \left(\frac{r - r_s}{R_0}\right)^2\right]. \tag{2}$$

We choose $k = 30\epsilon/\sigma^2$ and the maximum bond extension $R_0 = 1.5\sigma$, as in Ref. 35. We also incorporate a potential that promotes even spacing of strands on the surface of the core. Specifically, we use a three-body angular potential

$$U_{\mathrm{lin}}^{\mathrm{core}} = k_{\mathrm{lin}}^{\mathrm{core}}(1 + \cos\theta), \tag{3}$$

where θ is the angle defined by the first monomer of a pair of strands, with the NP core as the vertex. We choose a relatively large value $k_{\mathrm{lin}}^{\mathrm{core}} = 100$ to maintain a near uniform spacing of strands. We also considered $k_{\mathrm{lin}}^{\mathrm{core}} = 30$, and found only a minor quantitative difference in our results. Note that this potential does not keep the orientation of the strands fixed on the core, but rather allows strands to move along the surface of the core without detaching, introducing a "surface mobility" to the system. It has been shown that the surfaces of nanocrystals,[45] nanoparticles[46] and DNA-functionalized vesicles[47] can have significant mobility, which may have implications in DNA-linked crystal formation and stability, which we will examine later in this paper.

We study the model using molecular dynamics simulations with periodic boundary conditions. To control the temperature T, we use the Nosé-Hoover method.[48] The equations of motion are integrated using a two-level, three-cycle velocity-Verlet version of the rRESPA multiple time-step algorithm,[49] with the forces separated into rapidly-varying bonded forces and more slowly-varying non-bonded forces. The time step for the bonded forces is 0.002. For the remaining discussion, we use reduced units where length is given in units of the LJ length parameter σ and energy in units of LJ energy parameter ϵ. Temperature is expressed in units of ϵ/k_B, where k_B is the Boltzmann constant.

We study crystals with bcc or fcc symmetry consisting of 27 unit cells, which Ref. 35 showed is large enough to avoid finite size effects. Following Ref. 35, we examine fcc crystals in a single-component system in which all NPs are functionalized with the same DNA sequence (NP1-NP1 systems), and bcc crystals in binary systems in which there are two types of particles functionalized with complementary sequences (NP1-NP2 systems).[35] We functionalize particles with strands of DNA that are eight bases in length. Each strand has a two-base "spacer" region and a six-base "linker" region. We use the sequence NP-AAGGTACC for fcc systems, and the two sequences NP-TTTCTTCC and NP-AAGGAAGA for bcc systems. The sequences are chosen in such a way as to avoid binding of strands on the same core and to minimize partial binding with strands on other cores.

Since the spontaneous formation of crystal states is extremely slow, and in some cases not even accessible on the timescale of the simulation, we generate initial crystal configurations using knowledge of the crystal lattice

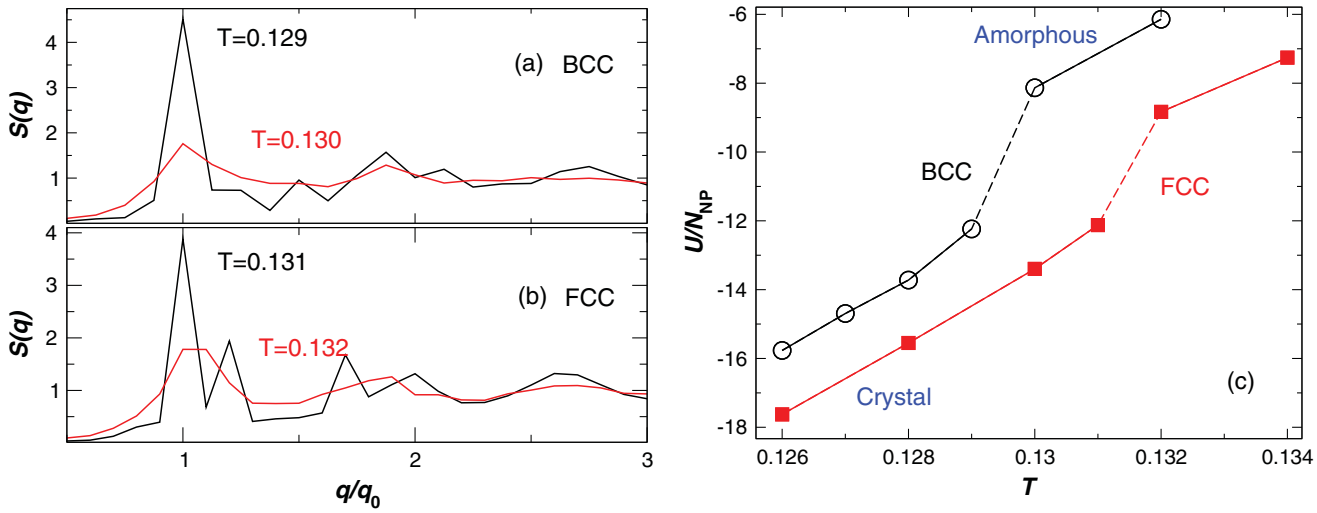

FIG. 2. Determination of the melting temperature T_M for crystals where the NP have $d = 2.8$ and 12 attached ssDNA, as in Ref. 35. The collapse of the Bragg peaks in the structure factor $S(q)$ of the (a) bcc and (b) fcc systems unambiguously indicates melting. Here, q_0 corresponds to the first peak of $S(q)$. (c) The melting transition is also apparent from the DNA base bonding energy U/N_{NP} on heating of the crystal. A jump in U/N_{NP} (dashed line) occurs upon crossing T_M.

parameters.[35] Since we prepare the initial configurations by hand, they are free from defects, such as positional permutations of the bcc lattice. We locate the melting temperature T_M by heating initially prepared crystal configurations. As shown previously, T_M obtained by this method coincides with the thermodynamic melting temperature for these systems.

III. EFFECTS ON CRYSTAL MELTING

A. Rigidity of attachment

When DNA strands are attached to a single spherical NP, the strands are able to move along the surface of the NP core without detaching (mobile-strand system). Examining the effects of mobility is relevant especially for DNA-functionalized vesicles;[47] additionally, atomic displacements at the NP surface are also possible.[46] This mobility is not present in the icosahedral core model[35] (immobile-strand system), so a comparison of the two systems allows us to determine the effect of surface mobility on the overall crystal stability. To isolate the effect of mobility alone, we compare icosahedral and spherical-core systems with the same core diameter $d = 2.8$ with 12 attached DNA strands. The core diameter of the icosahedral NP is given by that of the sphere circumscribing the icosahedron.

We determine T_M for the mobile-strand system from the collapse of the Bragg peaks in the static structure factor $S(q)$ (Figs. 2(a) and 2(b)). The static structure factor is the Fourier transform of pair correlation function $g(r)$. The melting transition also causes a jump in energy (Fig. 2(c)). Based on these data, fcc crystals formed in the immobile-strand system have a slightly larger T_M than fcc crystals formed in the mobile-strand system. The effect is quite weak, with T_M changing by only $\approx 1\%$. We can understand the sign of the difference based on the difference in the core NP symmetry. Specifically, the orientation of strands on the cores in the icosahedral immobile-strand system matches the symmetry of the fcc crystal. Therefore, bonds more readily form in the immobile-strand system than the mobile-strand system. The matching symmetry of the core NP and the fcc crystal stabilizes the crystal in the immobile-strand system relative to the mobile-strand system.

The change in T_M for the bcc crystal is opposite to that of the fcc, i.e., T_M of the bcc crystal formed in the immobile-strand system is lower than that of the mobile-strand system. As in the case of the fcc crystal, the effect is weak, with T_M increasing by $\approx 3\%$. We can again understand the sign of the difference from the symmetry difference of the core NP. Since the icosahedral core NP do *not* match the symmetry of the bcc crystal, not all strands are able to form bonds in the immobile-strand system. In contrast, strands can orient in a pattern more favorable for the bcc crystal in the mobile strand system. Quantitatively, this results in 13% fewer bonds in the immobile-strand system than the mobile-strand system. This is a difference of ≈ 1.6 linked strands per NP, and thus promotes a more stable bcc crystal in the mobile-strand system.

For longer strand lengths, the differences between rigid and mobile attachment systems should be less pronounced, since, as we approach the strand persistence length, the importance of the symmetry of the core attachment will be diminished. The primary finding is that the effect of mobility on T_M is relatively weak. This is further supported by simulations with a smaller $k_{\text{lin}}^{\text{core}} = 30$ to allow strands greater mobility; these simulations found T_M values nearly indistinguishable from the systems with $k_{\text{lin}}^{\text{core}} = 100$.

B. Number of attached strands

In this section, we compare T_M of bcc and fcc crystals with $N_s = 12$, 20, or 30 attached ssDNA and a core diameter $d = 5.8$. Using the known length per base of DNA, we can map between length and number of bases. Accordingly, this diameter corresponds to ≈ 2 nm, similar to the experiments

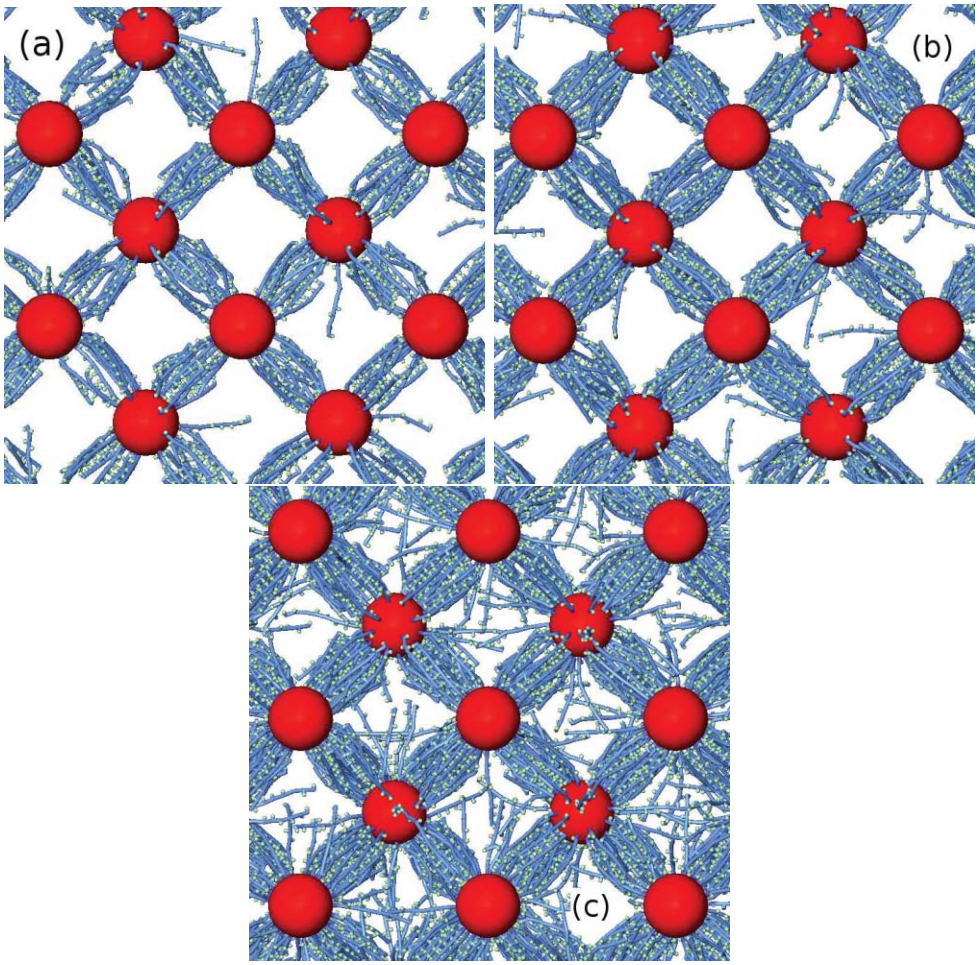

FIG. 3. Simulation snapshot of bcc crystals generated with core NP having $N_s = 12$, 20, or 30 attached ssDNA (a, b, and c, respectively).

of Ref. 50. We use a larger diameter than in Sec. III A, since the core NP surface area with $d = 2.8$ does not offer enough space to attach 20 or 30 strands. The effect of using different core sizes is examined in Sec. III C. The sequences are as previously described. Figure 3 shows example crystals from these simulations.

Figure 4 shows the variation of T_M with N_s. Generally, as N_s increases, multiple strands can make bonds between NPs. If the bonding of individual strand between NPs was purely independent, we would expect T_M have no dependence on N_s. Since T_M increases with increasing N_s, there is clearly cooperativity among strands linking NPs. For all systems, T_M of fcc crystals is larger than that of bcc crystals, presumably because fcc crystals have a coordination number of 12, while bcc crystals have a coordination number of 8. Accordingly, each NP in an fcc system has more nearest-neighbor particles with which to bind. Hence, more dsDNA is formed in fcc systems than bcc systems, leading to a larger T_M.

In Ref. 35, we showed that, for the case of 12 rigidly attached ssDNA, crystal melting was controlled by the DNA hybridization. To check if this is also the case when we vary N_s, we calculate the number of strands linking NPs immediately below and above T_M, and the resulting change in the number of linking strands on melting. To do so, we consider that two ssDNAs are linked when four or more (out of six possible) bases are linked. We say that two bases are linked if they are complementary to each other (A-T or C-G) and are within the range of attraction. Figure 5 shows the change in the number of linking strands on melting. For the $N_s = 12$ and 20 systems, the change is nearly constant (around 1.1 for fcc

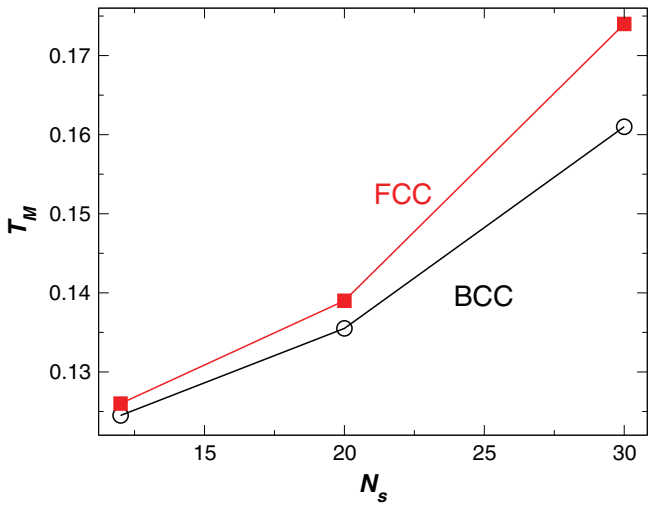

FIG. 4. Melting temperatures of bcc and fcc crystals with $N_s = 12$, 20, or 30 ssDNA and core diameter $d = 5.8$.

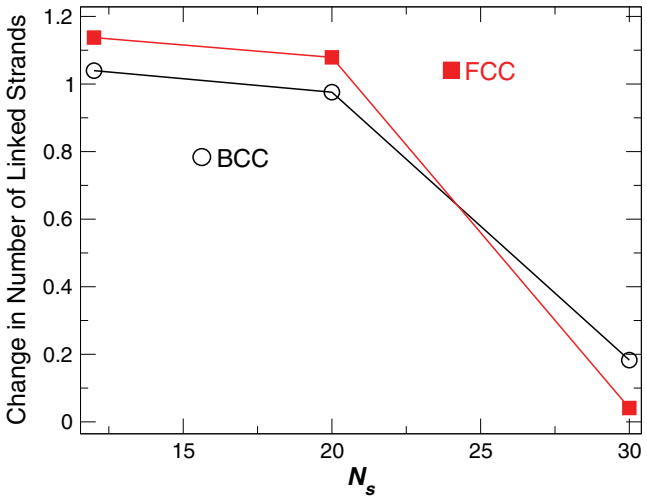

FIG. 5. Change in the number of linking strands per NP on melting the crystal. For $N_s = 12$ or 20, where hybridization dominates, melting results in the loss of ≈ 1 linking strand. For $N_s = 30$, this is not the case.

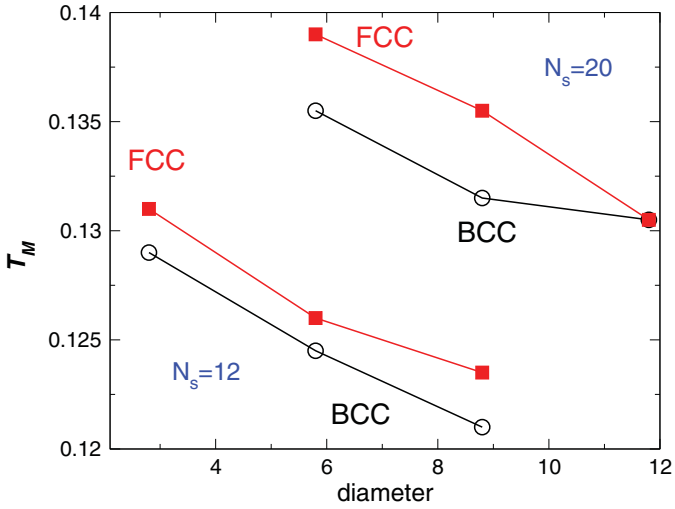

FIG. 6. T_M as a function of core diameter for $N_s = 12$ (lower left) and $N_s = 20$ (upper right).

and 1.0 for bcc) on melting. Accordingly, the unzipping of dsDNA controls the stability of the crystal for $N_s = 12$ and 20.

The results for $N_s = 30$ are in stark contrast. First, the fraction of bonded strands is nearly zero before melting. Consequently, the change in the number of bonded strands is also ≈ 0. Apparently, the crystal can remain stable simply from the crowding of non-bonded strands at larger N_s. Hence, the melting transition in this case is more due to a conformational shift in the NP crystalline structure than to the unzipping of dsDNA. Apparently, these crowded systems are more similar to attractive soft core NP.[36] This effect may be a consequence of the fixed density; if the system was allowed to expand, the NP might drift apart after strands unzip, reducing crowding effects of unzipped strands.

An obvious question is how our findings on the role of hybridization versus crowding compare with the melting of DNA-linked crystals in experiments where unzipping plays a dominant role in melting. To relate the experimental and simulated systems, we compare the relative density of DNA strands on the NP surface. The density of DNA strands on the NP surface in our simulations (with fixed diameter 5.8, ≈ 2 nm) ranges from ≈ 1.0 strands/nm^2 (for $N_s = 12$) to 2.4 strands/nm^2 (for $N_s = 30$). For experiments, the typical surface density is ≈ 0.1 strands/nm^2.[28,31,32] Hence, the experimental strand density is consistent with our findings in which hybridization dominates at densities $\lesssim 1.6$ strands/nm^2. Therefore, we will focus our remaining discussion on strand densities where DNA unzipping primarily controls crystal melting.

C. Core diameter and general model for melting temperature

In this section, we first examine systems with a fixed N_s and a variable core diameter d. We study six different systems: for $N_s = 12$ we examine $d = 2.8, 5.8,$ and 8.8, and for $N_s = 20$ we consider $d = 5.8, 8.8,$ and 11.8. As discussed previously, $d = 2.8$ does not have enough surface area for $N_s = 20$. These diameters correspond to an approximate experimental range of sizes from 1–4 nm. We exclude the $N_s = 30$ system, since the mechanism for melting there is not dominated by DNA hybridization. The sequences are the same as used in Secs. III A and III B.

Figure 6 shows that T_M decreases as d increases for both the $N_s = 12$ and the $N_s = 20$ systems. This finding is consistent with the experiments of Ref. 20, where it was found that increasing the core diameter lowered the temperature where amorphous aggregates melt. To understand this result, we need to consider the strain put on dsDNA links as the core size changes. Energetically, these links prefer to be nearly linear (for short strands). Hence, as the core diameter increases, any distortion of the crystal order puts a strain (more properly, a torque) on the dsDNA linkage, and this strain increases with increasing d. This effect was argued for in Ref. 35, where the effect of distortions on the energy change at melting decreases with increasing the core diameter d and spacer region length s, but Ref. 35 only examined the effect of variable s. Specifically, Ref. 35 proposed that

$$T_M = \frac{\Delta U(T_M)}{\Delta S(T_M)} = \frac{c_1 N_s \ell - c_2(s + d/2)}{N_s \ell}, \qquad (4)$$

where N_s is the number of strands attached to the NP surface, d is the NP diameter, ℓ and s are the number of bases in the linker and spacer region, respectively.

Our current data, from this section and Sec. III B, allow us to test the proposed dependence on both N_s and d. In Ref. 35, Eq. (4) was tested with nine systems each for the bcc and fcc lattices. We further test Eq. (4) using six more systems each for the bcc and fcc lattices evaluated here. Figure 7 shows that T_M is well described by this simple model for all values of d and N_s examined in this research, as well as the T_M obtained for all values of ℓ and s in Ref. 35.

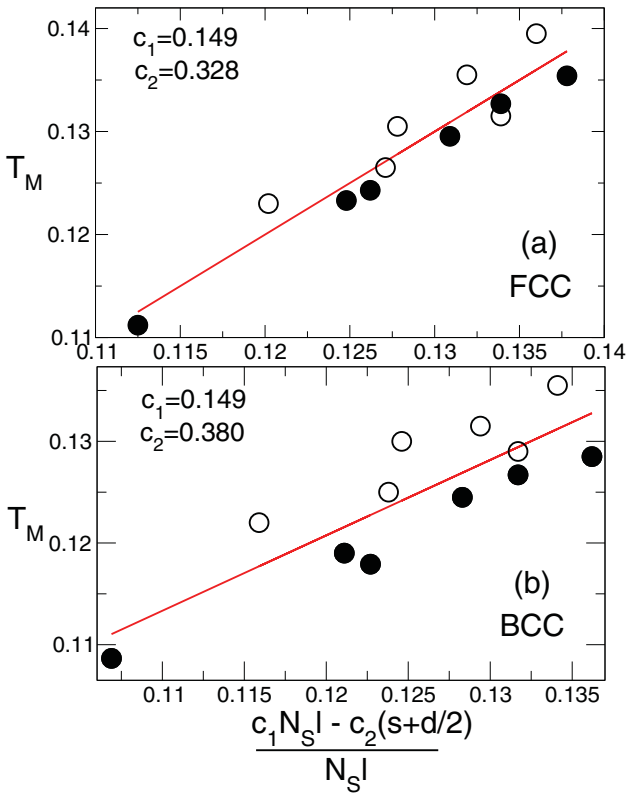

FIG. 7. Parametric plot of the numerical T_M as a function of the expected T_M from Eq. (4) for (a) fcc and (b) bcc lattices. The open symbols are the results from this work, while the filled symbols are from Ref. 35. The melting temperature is well described by the simple model of Eq. (4).

IV. CONCLUSION

Through use of a computational model, we have studied the effect of the number of attached strands and the core diameter on crystal stability. As we increase N_s while keeping the size of the NP fixed, T_M increases, which we attribute to the increased number of dsDNA linkages between NPs. Our results indicate that the melting transition of systems with $N_s = 12$ or 20 ssDNA is controlled primarily by the unzipping of strands, which destabilizes the crystal structure. For systems with $N_s = 30$, melting is controlled by crowding interactions of non-bonded strands, causing NP in such systems to act more like attractive ultra-soft core particles.[36]

These results have been obtained using a simulation incorporating DNA strand lengths much smaller than the persistence length of DNA, and NP which only interact through a repulsive soft-core potential. It is likely that systems with longer strand lengths and interacting core NP will be influenced differently by strand mobility, a variable number of strands, or a variable core size, and we intend to refine the coarse-grained model presented here to consider these factors in the future. Another important issue to address is the rate of crystallization, since kinetic constraints play a major role in successfully generating crystal states.[32,51] Finally, since DNA-functionalized NPs have the possibility to have complex phase diagrams with multiple interpenetrating phases,[38,41,52] it will be valuable to make a similar stability analysis for more exotic interpenetrating crystal states.

[1] C. Bustamante, S. B. Smith, J. Liphardt, and D. Smith, Curr. Opin. Struct. Biol. **10**, 279 (2000).
[2] N. C. Seeman, J. Theor. Biol. **99**, 237 (1982).
[3] N. C. Seeman, Nature (London) **421**, 427 (2003).
[4] A. Alivisatos, K. Johnsson, X. Peng, T. Wilson, C. Loweth, M. Bruchez, and P. G. Shultz, Nature (London) **382**, 609 (1996).
[5] C. Mirkin, R. Letsinger, R. Mucic, and J. Storhoff, Nature (London) **382**, 607 (1996).
[6] C. Niemeyer, Curr. Opin. Chem. Biol. **6**, 609 (2000).
[7] A. Condon, Nat. Rev. Genet. **7**, 565 (2006).
[8] V. T. Milam, A. L. Hiddessen, J. C. Crocker, D. J. Graves, and D. A. Hammer, Langmuir **19**, 10317 (2003).
[9] A. J. Kim, P. L. Biancaniello, and J. C. Crocker, Langmuir **22**, 1991 (2006).
[10] A. J. Kim, R. Scarlett, P. L. Biancaniello, T. Sinno, and J. C. Crocker, Nature Mater. **8**, 52 (2009).
[11] M. Valignat, O. Theodoly, J. Crocker, W. Russel, and P. Chaikin, Proc. Natl. Acad. Sci. U.S.A. **102**, 4225 (2005).
[12] P. Biancaniello, A. Kim, and J. Crocker, Phys. Rev. Lett. **94**, 0583021 (2005).
[13] P. Biancaniello, J. Crocker, D. Hammer, and V. Milam, Langmuir **23**, 2688 (2007).
[14] T. Schmatko, N. Geerts, E. Eiser, and W. Poon, Soft Matter **3**, 703 (2007).
[15] N. Geerts, T. Schmatko, and E. Eiser, Langmuir **24**, 5118 (2008).
[16] N. Geerts and E. Eiser, Soft Matter **6**, 4647 (2010).
[17] N. Geerts and E. Eiser, Soft Matter **6**, 664 (2010).
[18] Y. Maeda, H. Tabata, and T. Kawai, Appl. Phys. Lett. **79**, 1181 (2001).
[19] C. M. Soto, A. Srinivasan, and B. R. Ratna, J. Am. Chem. Soc. **124**, 8508 (2002).
[20] R. Jin, G. Wu, Z. Li, C. A. Mirkin, and G. C. Schatz, J. Am. Chem. Soc. **125**, 1643 (2003).
[21] S.-J. Park, A. A. Lazarides, C. A. Mirkin, and R. L. Letsinger, Angew. Chem. **40**, 2909 (2001).
[22] S. Park, A. Lazarides, J. Storhoff, L. Pesce, and C. Mirkin, J. Phys. Chem. **108**, 12375 (2004).
[23] S. Park, J. Lee, D. Georganopoulou, C. Mirkin, and G. Schatz, J. Phys. Chem. B **110**, 12673 (2006).
[24] P. Cigler, A. Lytton-Jean, A. Anderson, M. Finn, and S. Park, Nature Mater. **9**, 918 (2010).
[25] M. M. Maye, D. Nykypanchuk, D. van der Lelie, and O. Gang, J. Am. Chem. Soc. **128**, 14020 (2006).
[26] M. M. Maye, D. Nykypanchuk, D. van der Lelie, and O. Gang, Small **3**, 1678 (2007).
[27] D. Nykypanchuk, M. M. Maye, D. van der Lelie, and O. Gang, Langmuir **23**, 6305 (2007).
[28] D. Nykypanchuk, M. M. Maye, D. V. der Lelie, and O. Gang, Nature (London) **451**, 549 (2008).
[29] H. Xiong, D. van der Lelie, and O. Gang, Phys. Rev. Lett. **102**, 015504 (2009).
[30] D. Sun and O. Gang, J. Am. Chem. Soc. **133**, 5252 (2011).
[31] S. Y. Park, A. Lytton-Jean, B. Lee, S. Weigand, G. Schatz, and C. Mirkin, Nature (London) **451**, 553 (2008).
[32] R. Macfarlane, B. Lee, H. Hill, A. J. Senesi, S. Seifert, and C. Mirkin, Proc. Natl. Acad. Sci. U.S.A. **106**, 10493 (2009).
[33] J. Crocker, Nature (London) **451**, 528 (2008).
[34] J. Zheng, J. J. Birktoft, Y. Chen, T. Wang, R. Sha, P. E. Constantinou, S. L. Ginell, C. Mao, and N. C. Seeman, Nature (London) **461**, 74 (2009).
[35] F. Vargas Lara and F. W. Starr, Soft Matter **7**, 2085 (2011).
[36] C. N. Likos, H. Löwen, M. Watzlawek, B. Abbas, O. Jucknischke, J. Allgaier, and D. Richter, Phys. Rev. Lett. **80**, 4450 (1998).
[37] O.-S. Lee and G. C. Schatz, J. Phys. Chem. C **113**, 2316 (2009).
[38] C. W. Hsu, J. Largo, F. Sciortino, and F. W. Starr, Proc. Natl. Acad. Sci. U.S.A. **105**, 13711 (2008).
[39] C. W. Hsu, F. Sciortino, and F. W. Starr, Phys. Rev. Lett. **105**, 055502 (2010).
[40] J. Largo, F. W. Starr, and F. Sciortino, Langmuir **23**, 5896 (2006).
[41] W. Dai, C. W. Hsu, F. Sciortino, and F. W. Starr, Langmuir **26**, 3601 (2010).
[42] T. E. Ouldridge, I. G. Johnston, A. A. Louis, and J. P. K. Doye, J. Chem. Phys. **130**, 065101 (2009).
[43] F. W. Starr and F. Sciortino, J. Phys. Condens. Matter **18**, L347 (2006).
[44] J. Largo, F. W. Starr, and F. Sciortino, Langmuir **23**, 5896 (2007).
[45] P. L. Hansen, J. B. Wagner, S. Helveg, J. R. Rostrup-Nielsen, B. S. Clausen, and H. Topsoe, Science **295**, 2053 (2002).

[46]H. Zhang, P. Kalvapalle, and J. F. Douglas, Soft Matter **6**, 5944 (2010).
[47]P. Beales and T. Vanderlick, Biophys. J. **96**, 1554 (2009).
[48]D. Frenkel and B. Smit, *Understanding Molecular Simulation, Second Edition: From Algorithms to Applications Computational Science*, Vol. 1, 2nd ed. (Academic, New York, 2001)
[49]M. Tuckerman, B. J. Berne, and G. J. Martyna, J. Chem. Phys. **97**, 1990 (1992).
[50]J.-S. Lee, D. S. Seferos, D. A. Giljohann, and C. A. Mirkin, J. Am. Chem. Soc. **130**, 5430 (2008).
[51]W. Dai, S. Kumar, and F. W. Starr, Soft Matter **6**, 6130 (2010).
[52]C. W. Hsu and F. W. Starr, Phys. Rev. E. **79**, 041502 (2009).